signals can be obtained by substituting a glass test section and placing the probe outside. Interactions between the particles and the wall resulting in particle charging are difficult to rule out completely even though the metal wall was grounded.[1] However, this mechanism does not appear to be consistent with the results for the rarefaction wave since only a weak electrical signal was observed for this wave even though the velocity developed behind the wave is considerably greater than that behind the shock wave. We conclude that particles are charged by collisions in the flow behind the shock wave.

The mechanism for charging by interparticle collision may be discussed in terms of the following heuristic model. As explained by others,[2] particles of different sizes develop velocity lags behind the shock wave. If we use Stokes' drag law to estimate the aerodynamic force on a particle with radius r_i, then the particle's velocity U_i a distance X downstream of the shock is given approximately by

$$U_i = v_d + (v_u - v_d)\exp(-X/L_i) \quad (1)$$

when $|v_u - v_d| \ll v_d$. The upstream and downstream gas velocities are given by v_u and v_d, respectively, and L_i is the velocity equilibration length given by Marble[2] in the form

$$L_i = 2\rho v_d r_i^2/9\mu \quad (2)$$

where ρ is the density of particle material and μ is the gas viscosity. The maximum relative velocity between particles with radii r_1 and r_2 then occurs at a distance X_m downstream of the shock. X_m may be obtained from Eq. (1)

$$X_m = \frac{2\rho v_d r_1^2 r_2^2 \ln(r_1/r_2)}{9\mu(r_1^2 - r_2^2)} \quad (3)$$

Estimation of R, the rate of collisions per unit volume, for a simple single collision model yields

$$R = J_1 J_2 \pi (r_1 + r_2)^2 |(U_1 - U_2)/U_1 U_2| \quad (4)$$

where J_i is the ith particle flux. Thus, to the same order of approximation used above, the maximum collision rate occurs at X_m.

Collision can cause initially neutral particles to become charged as discussed by Kunkel[3] and an electric field would be produced as they separate after encounter. Since the maximum collision rate occurs downstream of the shock rather than at the discontinuity, the electric field would increase gradually as we have observed in these experiments. The same mechanism can occur in the case of the rarefaction wave but because of the decrease in particle density the resultant signals should be of a much smaller magnitude.

Temkin[4] has also examined particle collision in a comparable experiment. A suspension of droplets was subjected to repeated shock waves and droplet agglomeration as a result of collision was observed. A principal mechanical effect of collisions is to bring about momentum exchange between particles of different sizes as pointed out by Marble.[3] The importance of these works as well as the present study is to indicate some of the possible effects of interparticle collisions which have not been generally included in theoretical treatments of shock structure in particle suspensions.[5]

References

[1] Torobin, L. B. and Gauvin, W. H., "Fundamental Aspects of Solids-Gas Flow Part VI: Multiparticle Behavior in Turbulent Fluids," *The Canadian Journal of Chemical Engineering*, Vol. 39, No. 6, June 1961, pp. 113–120.

[2] Marble, F. E., "Mechanism of Particle Collision in the One Dimensional Dynamics of Gas Particle Mixtures," *The Physics of Fluids*, Vol. 7, No. 8, Aug. 1964, pp. 1270–1282.

[3] Kunkel, W. B., "The Static Electrification of Dust Particles on Dispersion into a Cloud," *Journal of Applied Physics*, Vol. 21, No. 8, Aug. 1950, pp. 820–832.

[4] Temkin, S., "Droplet Agglomeration Induced by Weak Shock Waves," *The Physics of Fluids*, Vol. 13, No. 6, June 1970, pp. 1639–1641.

[5] Kriebel, A. R., "Analysis of Normal Shock Waves in a Particle Laden Gas," *Transactions of the ASME, Ser. D: Journal of Basic Engineering*, Vol. 86, 1964, pp. 655–665.

Prediction of Nose Shape Effects on Nonlinear Stability Characteristics of Slender Cones

LARS E. ERICSSON* AND ROLF A. GUENTHER†
Lockheed Missiles & Space Company, Sunnyvale, Calif.

Nomenclature

C_{DN} = nose drag coefficient, $C_{DN} = D_N/(\rho U^2/2)(\pi d_N^2/4)$
C_m = pitching moment coefficient $C_m = M_p/(\rho U^2/2)(\pi d_B^3/4)$
d_B = base diameter
d_N = nose bluntness diameter
l = sharp cone length
q = rigid body pitch rate, $\dot{\alpha} = q$
U = velocity
x = axial body coordinate
$\Delta\bar{x}$ = cone center of gravity location forward of base
$\Delta\bar{x}_{CP}$ = cone center of pressure location forward of base
θ_c = cone frustum half-angle
θ_N = half-angle of conical tip
$\kappa_N, \bar{\kappa}_N$ = hypersonic scaling parameters for nose directing effects, defined in Eqs. (2) and (4)
ρ = air density
$\chi_l, \bar{\chi}_l$ = hypersonic scaling parameters for nosee drag effects, defined in Eqs. (1) and (3)
$C_{m\alpha}$ = static stability derivative, $C_{m\alpha} = \partial C_m/\partial\alpha$
$C_{mq} + C_{m\dot{\alpha}}$ = dynamice stability derivative, $C_{mq} + C_{m\dot{\alpha}} = \partial C_m/\partial(d_B\dot{\alpha}/U) + \partial C_m/\partial(d_B q/U)$

IT has been well domcumented that nose bluntness has a large effect on slender cone vehicle dynamics.[1-5] Only spherical nose bluntness has in general been investigated. Recently it has been shown that a change of nose shape from spherical to conical can change the vehicle characteristics substantially.[6,7] The conical nose tip geometry approximates the expected vehicle

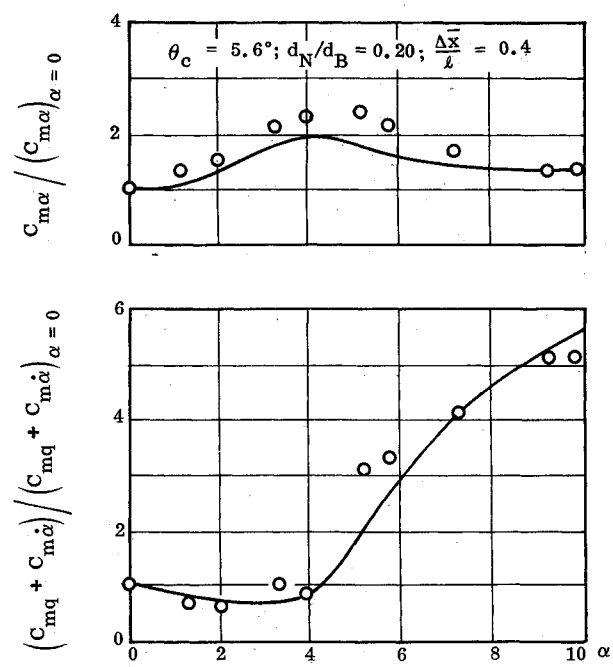

Fig. 1 Effect of angle of attack on the stability characteristics of a 20% blunt 5.6° cone with spherical nose bluntness.

Received February 9, 1972.
Index categories: Entry Vehicle Dynamics and Control; Nonsteady Aerodynamics; Supersonic and Hypersonic Flow.

* Senior Staff Engineer. Associate Fellow AIAA.
† Senior Aerodynamics Engineer.

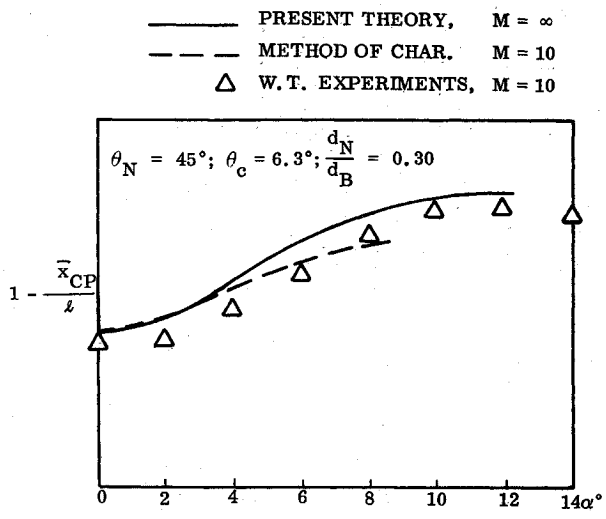

Fig. 2 Effect of angle of attack on center of pressure of a 30% blunt 6.3° cone with a 45° conical tip.

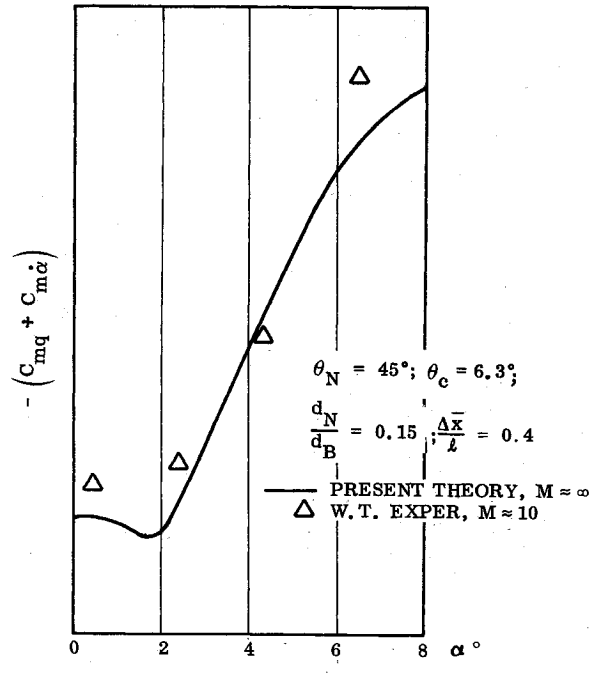

Fig. 3 Effect of angle of attack on the dynamic stability derivative of a 15% blunt 6.3° cone with a 45° conical nose tip.

nose shape after ablation under turbulent heating conditions. The present Note extends the analysis of nose shape effects at zero angle of attack[7] to include nonlinear effects of body attitude.

The nonlinear characteristics of spherically blunted cones have been shown to be well predicted by the analytic theory forming the basis for the present extension to conical nose shape effects[5] (Fig. 1). The equations for conical nose tips are developed in Ref. 7. The predictions of static and dynamic stability characteristics at moderate angles of attack agree well with wind-tunnel test results (Figs. 2 and 3).

When trying to utilize experimental data, one runs into one common problem: usually more than one of the significant parameters, i.e., cone angle, nose shape, bluntness ratio, and center of gravity, are changed between different tests. One needs scaling parameters that include the combined effects of several of the basic parameters. Such scaling parameters have been developed for the stability characteristics at zero angle of attack for spherical[6] and conical[7] nose bluntness. The effect of nose drag, i.e., the effect of an "Equivalent spherical" nose tip with attitude-insensitive drag, is scaled by the following parameter for arbitrary frustum cone angle

$$\chi_l = (\tan\theta_c/2)/(d_N/d_B)\,C_{DN}{}^{1/2} \tag{1}$$

This scaling parameter collapses the nose drag effects for conical nose tips (Fig. 4). The incremental change of the stability derivatives caused by a change of nose shape from spherical to conical is scaled by the following parameter

$$\kappa_N = -\tfrac{1}{2}\tan\theta_c/\tan\theta_N \tag{2}$$

The experimental results for a 50° conical nose tip[6] are well correlated by the scaling parameter κ_N (Fig. 5).

It was shown in Ref. 5 that the developed scaling laws for spherically blunted cones at $\alpha = 0$[8] could be extended to angle of attack by use of an effective tangent cone for the windward side[5]

$$\bar{\chi}_l = \chi_l[1+(8/3\pi)(\alpha/\theta_c)] \tag{3}$$

For small α (in comparison to θ_N) the scaling parameter κ_N, Eq. (2), could be extended similarly. That is

$$\bar{\kappa}_N = \kappa_N[1+(8/3\pi)(\alpha/\theta_c)] \tag{4}$$

Using these scaling parameters experimental stability data for blunted cones at $\alpha = 0$ can be used to obtain an approximate prediction of the nonlinear variation of stability derivatives with angle of attack. Let us assume that the data used in Fig. 4 were obtained experimentally. The data in Fig. 5 are experimental data, and if we had dynamic data a similar dynamic stability plot would also be available. In order to predict highly nonlinear dynamic stability characteristics, such as those in Fig. 3, we proceed as follows.

Compute effective scaling parameters $\bar{\chi}_l$ and $\bar{\kappa}_N$ using Eqs. (1–4). Enter Fig. 4b with $\chi_l = \bar{\chi}_l$ to get the effect of nondirecting nose bluntness, and in Fig. 5 use $\kappa_N = \bar{\kappa}_N$ to get the additional nose directing effect. This gives the nonlinear dynamic stability characteristics normalized to sharp cone values. It should be

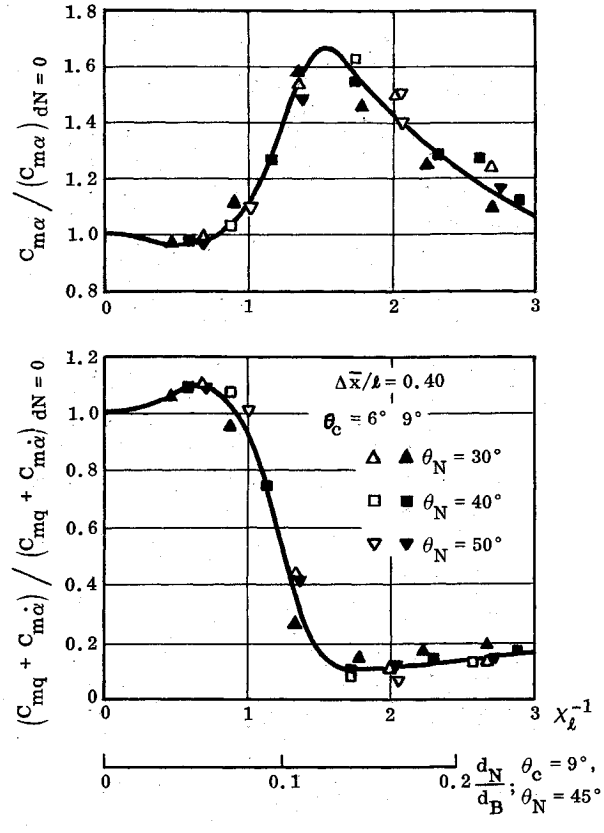

Fig. 4 Conical nose drag effect on stability characteristics of slender cones.

‡ The percentage change is 100 κ_N.

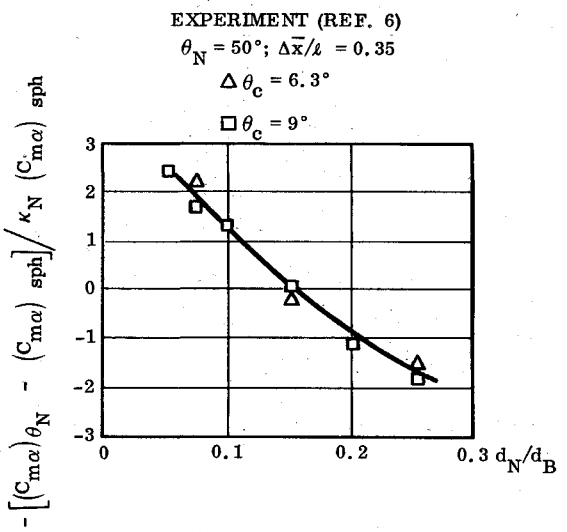

Fig. 5 Universal scaling of nose-tip directing ($C_{DN\alpha}$) effects for $\theta_N = 50°$.

emphasized that Fig. 4 can be defined using available data for spherically blunted cones. When the nose tip angle is not $\theta_N = 45°$ one has to determine the factor by which the nose-drag-induced loads obtained from Fig. 4 should be multiplied to give the complete loading on the frustum aft of a conical nose tip. Multiplying by the sharp cone values and adding the effect of nose tip lift (using modified Newtonian Theory, $C_{p\max} \approx 1.8$) would then give the sought prediction of experimental nonlinear characteristics. It should be emphasized that this whole procedure is valid only if the c.g. location in percent of sharp cone length remains the same.

Using Eq. (3) we find that the 6.3° cone at $\alpha = 3°$ would correspond to a 9° tangent cone at $\alpha = 0$, which in Fig. 4b places $d_N/d_B = 0.15$ right where the steep increase of dynamic stability will occur if the "effective cone angle" is increased further through increased angle of attack. This explains the steep increase of dynamic stability for $\alpha > 3°$ in Fig. 3.

References

[1] Walchner, O. and Clay, J., "Nose Bluntness Effects on the Stability Derivatives of Cones in Hypersonic Flow," *Transactions of the Second Technical Workshop on Dynamic Stability Testing*, Vol. 1, Paper 8, April 1965, Arnold Engineering Development Center, Arnold Air Force Station, Tullahoma, Tenn.

[2] Ward, L. K. Jr. and Uselton, B. L., "Dynamic Stability Results for Sharp and Blunt 10-Deg. Cones at Hypersonic Speeds," *Transactions of the 3rd Technical Workshop on Dynamic Stability Problems*, Vol. III, Paper 2, Nov. 1968, NASA Ames Research Center, Moffett Field, Calif.

[3] Malcolm, G. N. and Rakich, J. V., "Comparison of Free-Flight Experimental Results and Theory, on the Nonlinear Aerodynamic Effects of Bluntness for Slender Cones," *AIAA Journal*, Vol. 9, No. 3, March 1971, pp. 473–478.

[4] Rie, H., Linkievicz, E. A., and Bosworth, F. D., "Hypersonic Dynamic Stability, Part III, Unsteady Flow Field Program," FDL-TDR-64-149, Part III, Jan. 1967, Air Force Flight Dynamics Lab., Wright-Patterson Air Force Base, Chio.

[5] Ericsson, L. E., "Effect of Nose Bluntness, Angle of Attack, and Oscillation Amplitude on Hypersonic Unsteady Aerodynamics of Slender Cones," *AIAA Journal*, Vol. 9, No. 2, Feb. 1971, pp. 297–304.

[6] Neff, R. S., "Conical Nose Shape Effects on Drag and Stability at Mach 10," *Journal of Spacecraft and Rockets*, Vol. 9, No. 1, Feb. 1972, pp. 126–128.

[7] Ericsson, L. E. and Guenther, R. A., "Effect on Slender Vehicle Dynamics of Change from Spherical to Conical Nose Bluntness," *Journal of Spacecraft and Rockets*, Vol. 9, No. 6, June 1972, pp. 435–440.

[8] Ericsson, L. E., "Universal Scaling Laws for Hypersonic Nose Bluntness Effects," *AIAA Journal*, Vol. 7, No. 12, Dec. 1969 pp. 2222–2227.

Effect of Polarization on the Apparent Emittance of Rectangular Groove Cavities

C. L. TIEN*
University of California, Berkeley, Calif.

SEVERAL recent studies showed that the effect of polarization may become appreciable for radiant heat transfer among surfaces as a result of multiple reflections.[1-3] This effect is commonly neglected in evaluating the apparent emittance of surface cavities.[4,5] The present Note is to demonstrate the effect of polarization on the apparent emittance of rectangular groove cavities with specularly reflecting walls. It is also interesting to point out here that the present result is obtained directly from existing numerical results for long passage transmittance[2] through simple consideration.

Figure 1 shows a rectangular groove cavity with specularly reflecting walls. For convenience, consider $T_c > T_w$ and the radiant energy flux into the cavity is thus given by

$$q = \sigma(T_c^4 - T_w^4)\tau_{12} + \sigma(T_c^4 - T_w^4)\tau_{13} \tag{1}$$

where τ_{ij} is the transmittance between surfaces i and j. In accordance with the general definition of apparent emittance (or absorptance)[5]

$$\varepsilon = q/\sigma(T_c^4 - T_w^4) \tag{2}$$

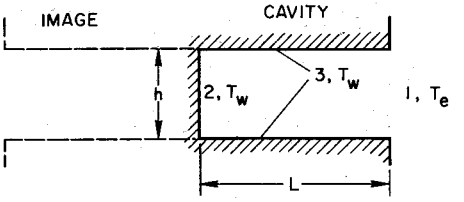

Fig. 1 Rectangular groove cavity.

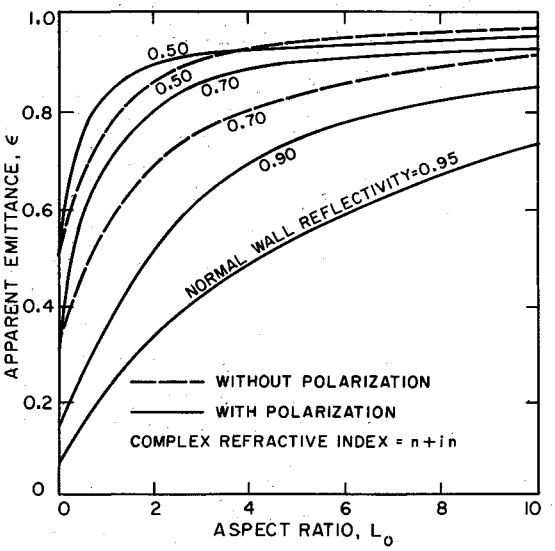

Fig. 2 Apparent emittance of rectangular groove cavities with specularly reflecting metallic walls.

Received February 18, 1972.
Index categories: Radiation and Radiative Heat Transfer; Thermal Surface Properties.

* Professor of Mechanical Engineering. Associate Fellow AIAA.